WACQT Lab Course 2021

Stockholm University - Trapped Ion Quantum Technologies

Supervisor -Markus Hennrich

This document is intended to provide a brief summary of several key concepts relevant to performing experiments on our ion trap system. It is not expected that everything should be fully understood prior to the lab course but reading through this document is recommended. For further reading, see the reference list included at the end of the instruction sheet.

1 Linear Paul Traps

A linear Paul trap uses a combination of dynamic and static electric fields in order to confine charged particles in 3D. A typical setup of electrodes is shown in figure 1. Confinement in the plane perpendicular to the blade electrodes (x-y in figure 1, from here on referred to as the radial direction) is provided by two electric quadrupole potentials, one which oscillates at radio frequencies and one which is static. Along the axis that runs parallel to the blade electrodes (z in figure 1, from here on referred to as the axial direction) a static field provides confinement between the two endcap electrodes. Close to the central axis of the trap the total trapping potential is described by

$$\Phi(\vec{r},t) = \frac{x^2-y^2}{2r_0^2}\left(V_0\cos(\Omega_{RF}t)+V_{of}\right) + \frac{\kappa}{2z_0^2}U_0\left(2z^2-x^2-y^2\right), \qquad x,y \ll r_0 \tag{1}$$

where V_0 is the oscillating voltage applied to the radial electrodes, V_{of} is the static offset voltage applied to the radial electrodes, U_0 is the static voltage applied to the endcaps, Ω_{RF} is the oscillation frequency of the dynamic radial quadrupole field, κ is a factor that depends on the specific trap geometry (≈ 0.042 for our trap design), r_0 is the distance between the radial electrodes and trap center and z_0 is the distance between the two endcap electrodes respectively.

By making the substitutions $\alpha = \frac{V_0}{2r_0^2}$, $\beta = \frac{\kappa U_0}{2z_0^2}$ and $\gamma = \frac{V_{of}}{2r_0^2}$ we can write an equation of motion for a particle of mass m and charge Q as

$$m\ddot{\vec{r}} = -Q\nabla\Phi(\vec{r},t) = -2Q\begin{pmatrix} x(\alpha\cos(\Omega_{RF}t)+\gamma-\beta) \\ -y(\alpha\cos(\Omega_{RF}t)+\gamma+\beta) \\ 2z\beta \end{pmatrix} \tag{2}$$

By making further substitutions the above equations of motion can be written in the form of Mathieu equations, which can then in turn be solved to find expressions for the trapping parameters $\omega_{x,y,z}$. We will not perform the full analysis here and will instead simply write out the substitutions a and q, which are known as stability parameters,

$$a_x = \frac{8Q(\gamma-\beta)}{m\Omega_{RF}^2}, \qquad a_y = -\frac{8Q(\gamma+\beta)}{m\Omega_{RF}^2} \qquad \text{and} \qquad q_x = -q_y = \frac{4\alpha Q}{m\Omega_{RF}^2}, \tag{3}$$

Successful trapping of a charged particle is only achieved for certain values of the stability parameters a and q, thus for a certain trap design the endcap and radial voltages as well as the oscillation frequency are tuned to provide stable confinement of particles of a certain charge-mass ratio. For a trap operating with the quadrupole potential described in equation 1 the motion of a charged particle at its center occurs in two forms: secular motion is a harmonic oscillation of the particle at frequencies $\omega_{x,y,z}$ and micromotion, which is a fast driven oscillation at the frequency of the quadrupole field

Ω_{RF}. The secular motional frequency is typically much smaller than Ω_{RF} and characterises the harmonic pseudo-potential in which the trapped particle is bound. Close to the trap center the 3D pseudo-potential takes the form

$$\Psi(x,y,z) = \frac{m}{2}(\omega_x^2 x^2 + \omega_y^2 y^2 + \omega_z^2 z^2), \tag{4}$$

and trapping frequencies $\omega_{x,y,z}$ can be derived from the aforementioned Mathieu equations.

$$\omega_{x,y} = \frac{\Omega_{RF}}{2}\sqrt{\frac{q_{x,y}^2}{2} + a_{x,y}} \qquad \text{and} \qquad \omega_z = \sqrt{\frac{4Q\beta}{m}}. \tag{5}$$

Generally for linear Paul traps $r_0 \ll z_0$ and $a \approx 0$, following this approximation we often operate our trap with $q \approx 0.3$ and $\Omega_{RF} = 18.4$MHz which leads to typical trapping frequencies of $\omega_{x,y} \sim 2\pi \times 1.7$MHz and $\omega_z \sim 2\pi \times 840$kHz. Note that a is required to be non-zero to lift the degeneracy between the two radial modes, from the definitions in equation 6 it can be seen that the difference between a_x and a_y depends primarily on the factor γ, which in turn is tuned by the strength of the static quadrupole field V_{of}, typically we apply this offset using a stable battery voltage of 1.5V, corresponding to a radial splitting of $\sim$ 70kHz between the two modes.

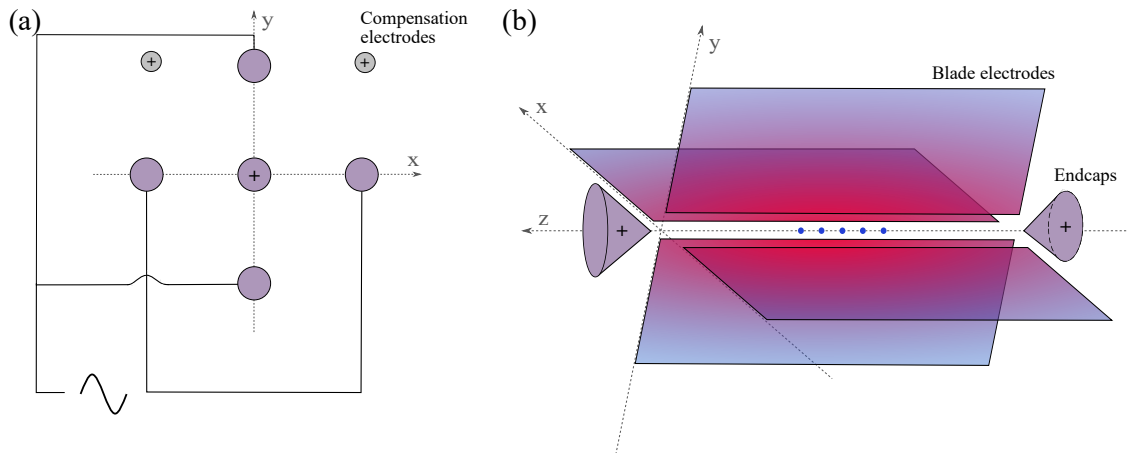

Figure 1: Trap electrode geometry: (a) Schematic showing how the radiofrequency quadrupole trapping fields are generated. DC voltages are applied to sets of compensation electrodes (shown in grey) to make small adjustments to the ion's position at the trap center. (b) Schematic of a typical "Innsbruck" design linear Paul trap with four radial electrodes spaced equidistant from one another in the x-y plane and two endcap electrodes spaced apart in the z-direction.

2 Laser-Ion Interaction

All of the key processes in our experimental setup make use of the interaction between an atom and a coherent light beam; we use lasers for cooling, state detection and almost all possible single- and multi-qubit operations. The single ion can be approximated as a composite quantum object consisting of a simple two-level system and a quantum harmonic oscillator; the former describes the state of the atom's outermost electron being either in the ground state $|g\rangle$ or an excited state $|e\rangle$, the latter describes the ion's secular motion at frequency $\omega_{x,y,z}$. Considering the light field as a monochromatic plane wave, we can describe the full Hamiltonian of the interacting system with three terms, describing the ion's internal electronic state, the ion's motional state and the interaction of the ion with the incoming laser light respectively.

$$\hat{H}_e = \frac{1}{2}\hbar\omega_{eg}\hat{\sigma_z}, \tag{6}$$

$$\hat{H}_m = \hbar\omega_{x,y,z}(\hat{a}^\dagger\hat{a} + \frac{1}{2}), \tag{7}$$

$$\hat{H}_{int} = \frac{1}{2}\hbar\Omega(\hat{\sigma}^+ + \hat{\sigma}^-)(e^{i(\omega_l t - \vec{k_l}\vec{r})} + e^{-i(\omega_l t - \vec{k_l}\vec{r})}), \tag{8}$$

where ω_{eg} and ω_l are the characteristic frequencies of the transition and laser light respectively, $\hat{\sigma_z}$ is the Pauli spin operator for the principal axis, $\hat{\sigma^+}$ and $\hat{\sigma^-}$ are the Pauli raising and lowering operators respectively, $\vec{k_l}$ is the wavenumber of the laser light, $\hat{r}$ is the position operator and Ω is the Rabi frequency - a measure of the strength of the incoming light field with respect to a certain transition. $\hat{a}^\dagger$ and $\hat{a}$ are the creation and annihilation operators of the ion motion. The interaction Hamiltonian is valid under the assumption that the laser is resonant with only a single transition.

The interaction Hamiltonian from equation 11 is simplified by making a rotating wave approximation, mapping from the Schrödinger to the interaction picture and defining the Lamb-Dicke parameter

$$\eta = k_l \cos\theta\sqrt{\frac{\hbar}{2m\omega}}. \tag{9}$$

The angle θ is between the direction of the laser beam and the ion's oscillatory motion, we can therefore define individual parameters for the x, y and z directions. The Lamb-Dicke parameter is an important quantity that defines how easily a laser can couple the ion's electronic and motional states. The coupling arises during absorption and emission processes due to the fact that momentum must be conserved. Utilising this coupling allows for laser cooling schemes and numerous multi-qubit gate operations to be employed in a trapped ion setup. The interaction Hamiltonian can then be written in terms of both Pauli raising/lowering operators for the electronic state and annihilation/creation operators for the motional quanta,

$$\hat{H}_I = \frac{1}{2}\hbar\Omega(\hat{\sigma}^+ e^{-i\Delta t}e^{[i\eta(\hat{a}^\dagger e^{i\omega_x t} + \hat{a}e^{-i\omega_x t})]} + h.c.), \tag{10}$$

where $\Delta = +\omega_l - \omega_{eg}$ is the detuning of the laser and $h.c.$ is the hermitian conjugate. If we first consider only the electronic states, the above Hamiltonian drives sinusoidal oscillations between the states $|g\rangle$ and $|e\rangle$. If we observe the action of this Hamiltonian over time we will see how population evolves between the ground and excited states at a characteristic frequency, which is the Rabi frequency Ω,

$$\Omega = \frac{\vec{d}_{g,e}\vec{E}_0}{\hbar}. \tag{11}$$

Here $\vec{d}_{g,e}$ is the transition dipole moment for the two states that are resonantly coupled to the laser and $\vec{E_0}$ is the vector electric field amplitude. Note here that $\Omega \propto \sqrt{I_0}$ where I_0 is then the intensity of the incoming laser light.

To determine the action of the above Hamiltonian on the ion's motional state we can perform a further approximation; assuming the following condition is met

$$\eta^2(2n+1) \ll 1, \tag{12}$$

where n is used here to denote the phonon occupation number for a particular motional mode. Under such circumstances the system is said to be in the Lamb-Dicke regime in which the coupling between the ion's electronic and motional states is sufficiently weak that transitions which change the motional quantum number n by more than ± 1 are strongly suppressed. Entering the Lamb-Dicke regime before performing quantum operations is an essential requirement in most ion trap systems, especially when geared towards quantum computation and quantum metrology. Physically, the above expression describes a system in which the extent of a trapped ion's oscillatory motion is small compared to the wavelength of the incoming light, such that Doppler effects caused by the relative motion are negligible. Instead, in the ion's rest frame it sees the incoming light at frequency ω_l modulated at the secular motional frequencies $\omega_{x,y,z}$ of its bound motion. Absorption at these sideband frequencies $(\omega_l \pm \omega_{x,y,z})$ necessitates the addition/subtraction of one phonon to/from the relevant motional mode. Along with the fact that spontaneous emission in the Lamb-Dicke regime primarily occurs via transitions that leave the phonon occupation number unchanged, these sideband transitions can be used to manipulate the motional state of the ion to perform resolved sideband cooling to the motional ground state or prepare specific phonon Fock states.

The Hamiltonian in equation 13 is then simplified based on which kind of transition is being driven. For the case where $\Delta = 0$ the laser drives the carrier transition $|g,n\rangle \leftrightarrow |e,n\rangle$ as per the interaction Hamiltonian

$$\hat{H}_{I_{carrier}} = \frac{1}{2}\hbar\Omega_{n\to n}(\hat{\sigma}^+ + \hat{\sigma^-}), \tag{13}$$

where $\Omega_{n\to n}$ is the phonon-number dependant coupling strength

$$\Omega_{n\to n} = (1-\eta^2 n)\Omega_0. \tag{14}$$

In the above expression Ω_0 is the coupling strength of the $(n=0) \leftrightarrow (n=0)$ transition (which is equivalent to the general Rabi frequency denoted simply as Ω in previous equations). For the case where $\Delta = -\omega_x$ the laser drives the red sideband transition $|g,n\rangle \leftrightarrow |e,n-1\rangle$ as per the interaction Hamiltonian

$$\hat{H}_{I_{red}} = \frac{1}{2}i\hbar\Omega_{n\to n-1}(|e,n-1\rangle\langle g,n| - |g,n\rangle\langle e,n-1|) \tag{15}$$

with coupling strength

$$\Omega_{n\to n-1} = \eta\sqrt{n}\Omega_0. \tag{16}$$

For the case when $\Delta = +\omega_x$ the laser drives the blue sideband transition $|g,n\rangle \leftrightarrow |e,n+1\rangle$ as per the interaction

Hamiltonian

$$\hat{H}_{I_{blue}} = \frac{1}{2}\hbar\Omega_{n\to n+1}(|e,n+1\rangle\langle g,n| - |g,n\rangle\langle e,n+1|) \tag{17}$$

with coupling strength

$$\Omega_{n\to n+1} = \eta\sqrt{n+1}\Omega_0. \tag{18}$$

The three types of transitions are shown in figure 2 below. Note that the dependence of the Rabi frequency on the phonon occupation number n differs for the three different transitions, this means we can compare the observed Rabi frequencies (whilst keeping the strength of the laser constant) as a method to measure the temperature of the ion whilst in the Lamb-Dicke regime. To measure the temperature of an ion that has not been cooled to a specific motional Fock state, for example, whilst the ion remains in a thermal state after Doppler cooling, we can use the fact that uncertainty in the motional state leads to rapid dephasing when driving Rabi oscillations on the carrier transition. The evolving population is then well described by the approximation

$$p_e(t) \approx \frac{1}{2}\left\{1 - \frac{\cos 2\Omega t + 2\Omega t\eta^2(\tilde{n}+1)\sin 2\Omega t}{1+(2\Omega t\eta^2(\tilde{n}+1))^2}\right\}. \tag{19}$$

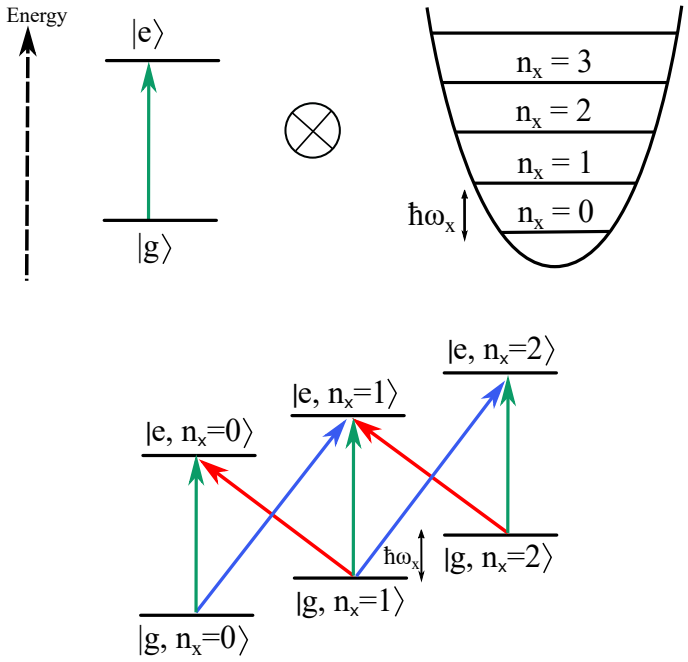

Figure 2: (Top) Composite quantum system for a single trapped ion, consisting of a simple two-level system and a quantum harmonic oscillator. (Bottom) The two can be coupled by laser light driving transitions at particular sideband frequencies.

3 Bloch Spheres and Ramsey Sequences

The evolution of the state of a two-level quantum system can be easily demonstrated using the Bloch sphere. For the ground and excited states $|g\rangle$ and $|e\rangle$ we can create a Bloch sphere as depicted in figure 3. The state vector on this Bloch sphere represents the electronic state of a single trapped ion, interaction with a near resonant light field will cause the state vector to be rotated about a certain axis by a certain angle. The axis of rotation is determined by the phase and detuning of the laser with respect to the atomic transition. Typically we consider the Bloch sphere in the rotating frame of the transition's characteristic frequency ω_{eg}, assuming $\Delta = \omega_l - \omega_{eg} = 0$ the axis of rotation must lie in the plane of the equator and is determined by the relative phase between the laser and ion. If $\Delta \neq 0$ the rotation axis is tilted additionally towards the poles so that the state vector no longer rotates over the course of a great arc on the surface of the sphere, the result is a faster but less efficient population transfer.

The rotation angle is determined by the area of the incoming light pulse, we define an area that transfers population directly from $|g\rangle$ to $|e\rangle$ and vice versa as a π pulse (this is the equivalent of an X-gate when referring to logical qubit states). Note that the pulse area depends on both the power and length of the pulse, thus for a particular Rabi frequency, which defines the rate at which we perform one full cycle around the Bloch sphere, we can tune a π pulse by setting the length to $t = \frac{1}{2\Omega}$. We can similarly define $\frac{\pi}{2}$ pulses that allow us to form superpositions of $|g\rangle$ and $|e\rangle$ (the equivalent of a Hadamard gate for logical qubit states).

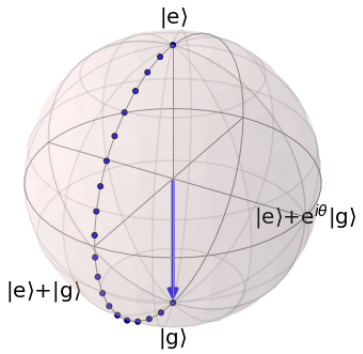

Figure 3: Bloch sphere representation of a single ion initialised in the ground state, the blue dots represent one possible path that the state vector could take under the action of a π pulse.

One of the ways in which the Bloch sphere picture is particularly useful is when performing Ramsey experiments. Such pulse sequences are invaluable in trapped ion experiments and can be used to estimate coherence times, investigate noise sources and perform highly precise measurements of atomic transition frequencies. The basic sequence of a Ramsey experiment is shown in figure 4. Prominent sources of phase noise will affect the outcome of the sequence since repeat experiments will not necessarily have the state vector evolving uniformly around the equator of the Bloch sphere, thus causing dephasing. The longer the interrogation time between pulses the more sensitive we become to such phase noise, until the dephasing becomes too severe and coherence between the two states is lost.

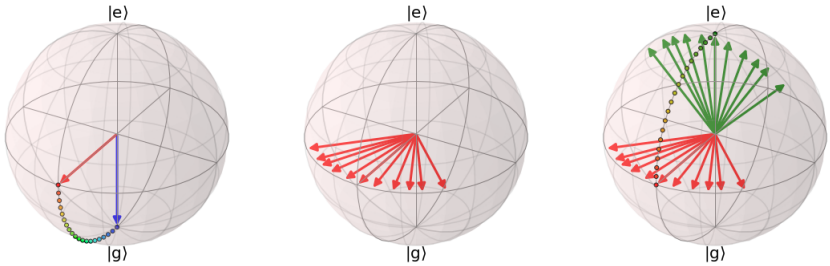

Figure 4: The Ramsey sequence is broken down into three steps, here they are depicted after the ion has been initialised in the ground state. (1) A $\frac{\pi}{2}$ pulse brings the state vector to an equal superposition of $|g\rangle$ and $|e\rangle$. (2) The laser is switched off for an interrogation time τ, during which the state vector will precess about the polar axis if the system is disturbed by external sources of phase noise. (3) A second $\frac{\pi}{2}$ is applied at the end of the interrogation time, the final position of the state vector depends on the phase accumulated during the time τ.

One method in which we can extend the coherence time of the system whilst performing a Ramsey sequence is to include a Hahn spin echo pulse during the wait time. The spin echo sequence is shown in figure 5 below.

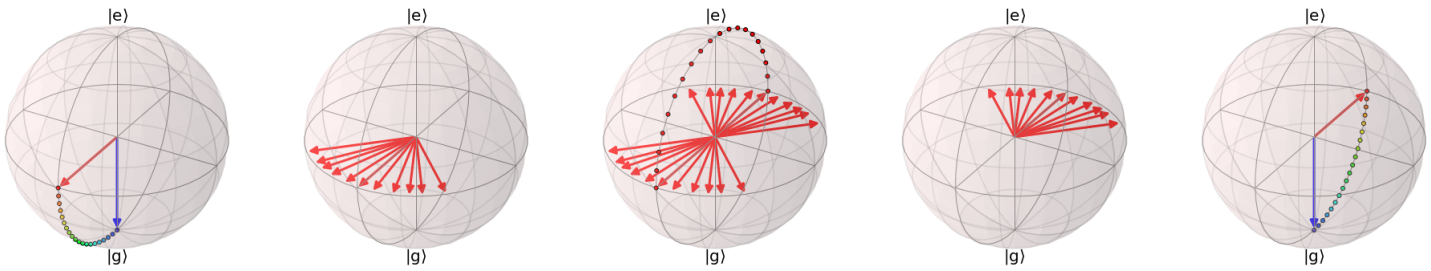

Figure 5: The spin echo pulse is embedded into a Ramsey sequence and allows the system to self-compensate for the effects of dephasing up to a certain level. The initial steps are the same as in the ordinary Ramsey sequence, however during the interrogation time, at $t = \frac{\tau}{2}$ a π is applied that inverts the state vector, the system is then allowed to evolve just as before for another time $\frac{\tau}{2}$ before the second $\frac{\pi}{2}$ pulse is applied. Any phase accumulation that occurs before the spin echo pulse is then compensated after the pulse as the phase continues to evolve in the opposite direction, thereby realigning along the axis that the state was initially transferred to.

4 Experimental setup

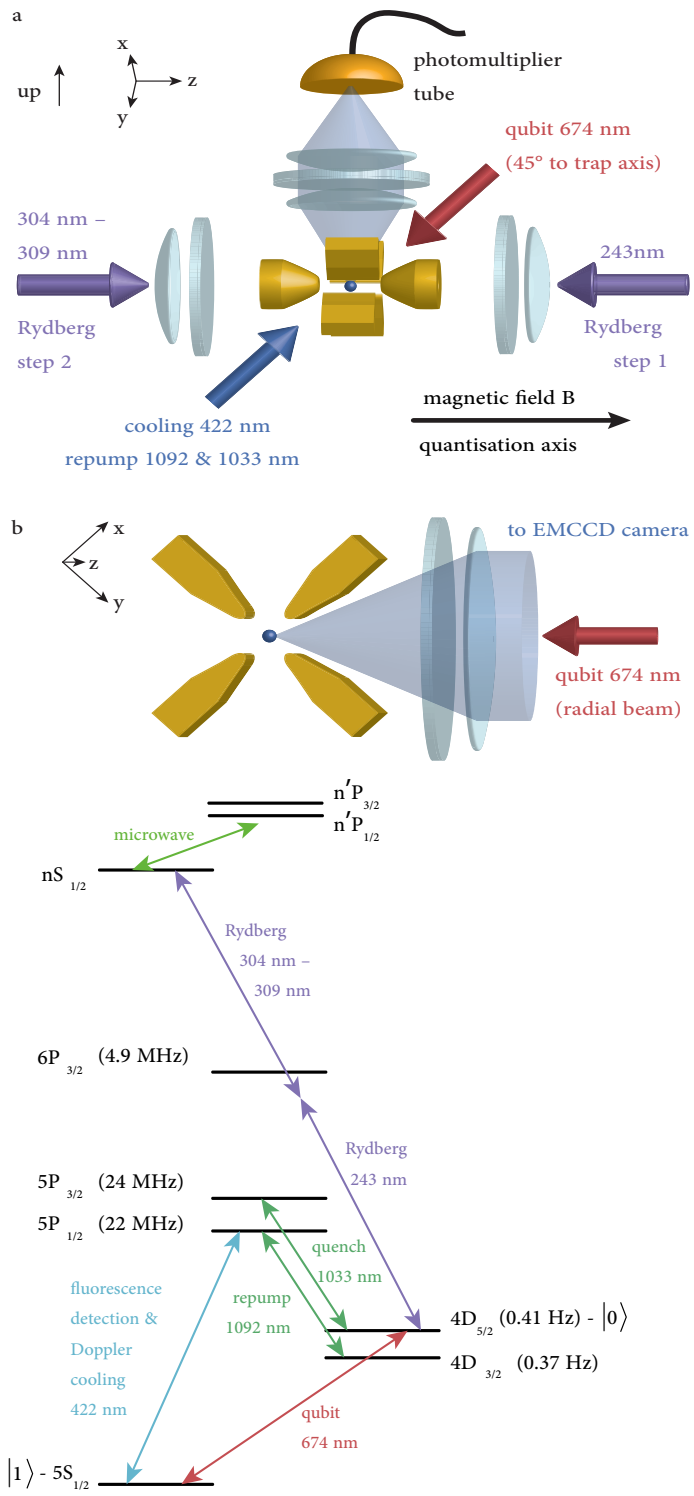

The experimental setup consists of a single Innsbruck-design ion trap mounted in a vacuum-sealed chamber. We use 9 different laser systems for various purposes, including qubit manipulation, cooling and state detection. The latter is performed by shining light at 422nm at the centre of the trap. If the ion is in the ground state $5S_{1/2}$ the 422nm light drives population to the short-lived excited state $5P_{1/2}$. Thus if the ion is in the ground state $5S_{1/2}$ when a measurement is performed the population will be transferred up and then rapidly decay back down before being excited again. A fraction of the spontaneously emitted photons that are produced during the thousands of excitations that occur each second are focused onto either a PMT or EMCCD camera that are capable of amplifying the weak signals that they receive.

If a pulse is performed with the 674nm qubit laser after initialising in the ground state, population is transferred from $5S_{1/2}$ to $4D_{5/2}$. Due to the transition being dipole-forbidden the lifetime of the excited state is significantly longer and a measurement performed will show a lack of counts above the background noise on both the PMT and EMCCD signals, since there is no longer any population to excite from the ground state.

Ions are loaded into the trap by ablating a small sample of Sr and using two lasers to photo-ionise the atoms that are blasted off of the sample surface. Ions passing close to the trap centre are then caught by the electric fields and cooled using red-detuned light at 422nm. Both optical pumping for ground state initialisation and sideband cooling to the motional ground state are performed using pulses on the 674nm qubit laser.

Figure 6: (Top) Schematic of the ion trap including optical access ports and state detection scheme. (Middle) Schematic of radial electrodes along the trap axis as well as secondary system for fluorescence detection. (Bottom) Simplified energy level scheme for $^{88}Sr^{+}$

Useful literature:

Linear Paul traps - https://www.quantumoptics.at/images/publications/dissertation/roos_diss.pdf (p.5-8)

Lamb-Dicke regime - https://www.quantumoptics.at/images/publications/dissertation/roos_diss.pdf (p.15-16)

Doppler Cooling - https://www.quantumoptics.at/images/publications/dissertation/roos_diss.pdf (p.19-21)

Sideband Cooling - https://www.quantumoptics.at/images/publications/dissertation/roos_diss.pdf (p.21-22)

Rabi oscillations and temperature measurement -https://www.escholarship.org/content/qt2nv876dw/qt2nv876dw.pdf (p.10-13)

Bloch sphere rotation - https://atomoptics-nas.uoregon.edu/~dsteck/teaching/quantum-optics/quantum-optics-notes.pdf (p.169-172)